INDIRECT ESTIMATION OF BUILDING FLOORS USING AERIAL PHOTOGRAMMETRY AND STREET-LEVEL 360° IMAGERY FOR SEISMIC RISK ASSESSMENT

ESTIMACIÓN INDIRECTA DEL NÚMERO DE PISOS EN EDIFICACIONES USANDO FOTOGRAMETRÍA AÉREA E IMÁGENES PANORÁMICAS 360° A NIVEL DE CALLE PARA LA EVALUACIÓN DEL RIESGO SÍSMICO

Jhianpiere Stainer Salinas Villar[1*], Angel Martin Quesquen Ramirez[1], Fernando Garcia Bashualdo[1], Miguel Augusto Diaz Figueroa[1, 2], Sergio Manuel Isuhuaylas Aguirre[1], Miguel Luis Estrada Mendoza[1], Carlos Alberto Zavala Toledo[1]

[1] *Japan-Peru Center for Earthquake Engineering Research and Disaster Mitigation, National University of Engineering, Lima, Peru*

[2] *Faculty of Civil Engineering, National University of Engineering, Lima, Peru*

Received (Recibido): 13 / 03 / 2025 Publicado (Published): 30 / 12 / 2025

RESUMEN

El levantamiento de información de edificaciones es un componente clave en la planificación urbana y la gestión del riesgo de desastres. En este estudio, se comparan dos métodos semiautomatizados para la estimación del número de pisos de edificaciones: uno basado en imágenes aéreas capturadas con drones y otro a partir de imágenes 360° obtenidas de Google Street View. Para el método fotogramétrico, se generaron modelos tridimensionales y productos fotogramétricos generados a partir de imágenes aéreas. Los resultados mostraron que la precisión en la estimación del número de pisos alcanzó su mayor valor en edificaciones de un solo piso (92%) y el menor en edificaciones de cinco pisos (66%). En el caso del análisis con imágenes 360°, únicamente usando los modelos de clasificación se obtuvo una precisión de más del 0.80% para todas las clases propuestas, aunque con la limitación que no identifica lotes baldíos ni edificaciones mayores a 5 de manera exacta. Asimismo. se implementaron diversos modelos de aprendizaje automático, los cuales, tras la evaluación del desempeño, el modelo Random Forest obtuvo la mejor precisión con un valor de 0.861.

Palabras Clave: Estimación de pisos de edificaciones, nDSM, riesgo sísmico, aprendizaje profundo, imágenes 360

ABSTRACT

Building data collection is a key component of urban planning and disaster risk management. In this study, two semi-automated methods for estimating the number of floors in buildings are compared: one based on aerial images captured by drones, and another using 360° images obtained from Google Street View. For the photogrammetric approach, three-dimensional models and photogrammetric products were generated from aerial images. The results showed that accuracy in floor estimation was highest for single-story buildings (92%) and lowest for five-story buildings (66%). Regarding the analysis using 360° images, classification models alone achieved an accuracy greater than 80% for all proposed classes, although they exhibited limitations in accurately identifying vacant lots and buildings taller than five floors. Additionally, several machine learning models were implemented, among which the Random Forest model achieved the highest accuracy, with a value of 0.861.

Keywords: Building floor estimation, nDSM, seismic risk, seismic risk, 360 imageries.

1. INTRODUCTION

Building height is a primary parameter of characterization for different objectives and research workflows. The state of the art for estimating it is very extensive in both direct and indirect methods. While first focus on using equipment that employs laser [1, 2, 3], Global Navigation Satellite System (GNSS) technologies or optical observations assisted by humans [4] ; the indirect methods is based on the application of topics like remote sensing: satellite images [5], Remotely Piloted Aircraft (RPA) images [6, 7, 8] ; deep learning and neuronal networks [9, 10, 11].

[1] * Corresponding author:
E-mail: jsalinas@uni.pe

Current Peruvian seismic risk assessment and tsunami hazard methodologies are applying at block level and use the building height as one of its parameters [12, 13]; so, this study open a more detailed evaluation, approaching many difficulties previously described.

Additionally, building height information is crucial for determining debris volume and planning its removal after a disaster caused by a natural or anthropogenic hazard [14, 15, 16]. Moreover, these results would help identify buildings with a high potential for collapse during a major earthquake, whose debris could obstruct pedestrian and/or vehicular evacuation.

Aerial images are used for the 3D reconstruction of the surface (including topography and objects on it) through photogrammetry. Technological advancements have now made it possible to use drones to capture high-resolution aerial images. This approach combines the versatility of unmanned aerial vehicles (UAVs) with modern digital processing techniques, enabling the efficient generation of 3D point clouds and digital elevation models (DEMs) with exceptional precision and detail. Specifically, the use of drones has revolutionized traditional methods for structure reconstruction and detection, offering more cost-effective, efficient, and faster alternatives compared to systems such as LiDAR and other conventional techniques [17].

Among the most relevant products generated through photogrammetry, Digital Surface Models (DSMs) are crucial for representing the vertical elevation of the terrain and the structures present on it. Normalized DSM (nDSM), derived through morphological operations such as the "top-hat" technique, allow for the estimation of the relative height of objects above the ground, making them particularly useful for building detection and analysis, a reference regarding the use of this photogrammetric product was made by [18] where it reports high accuracy in building detection through the use of elevation information from the nDSM.

Based on elevation model data, Erener [1] presents a workflow for calculating the number of floors using the nDSM value, generated by LiDAR, located at the centroid of each building trace and dividing it by the average building floor height (taken as 3 m).

Another recent application of remote sensing in the field of building height extraction was conducted by [7], using satellite imagery and implementing photogrammetry and deep learning for the generation of elevation models, as well as the use of the percentile value for height determination. Some of fields that require building height are land use, urban planning and building construction.

These methods need a 360-magery dataset so there are some popular GeoServices that provide a large amount of data such as Google Street View, Mappilary, Open Street View, Baidu, etc. Many of them provides API's for extracting data through an automized request process, but all is not free licensed.

However, Peru as a country with a bad urban planification even in its capital, so it's a challenger study area for replicating these methods, as buildings are very close to each other and there are no clear boundaries between them, poorly georeferenced cadastre maps at the lot level provided by the government; low-quality and expensive satellite imagery; visual pollution, etc.

This research compares two of the most principal indirect methods, one through aerial images and another through 360 images at street level.

2. METODOLOGY

2.1. BUILDING HEIGHT ESTIMATION THROUGH PHOTOGRAMMETRIC RESTITUTION

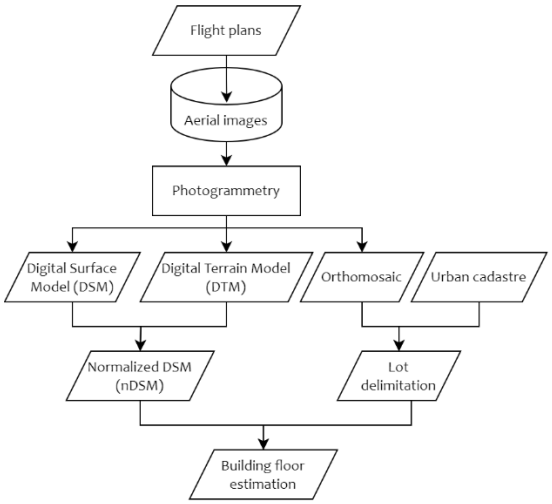

Fig. 1. The framework of the building heights and floor estimation method.

2.1.1. PHOTOGRAMMETRIC FLIGHT PLANS

Flight plans were developed for the capture of aerial photographs in the study area to obtain information on all the infrastructure present in the flight area and thus estimate the height of the buildings detected.

The flight was made at an average altitude of 50 meters achieving an average GSD of 3 cm which

guarantees a high definition of the photogrammetric products that will be used in this research.

The equipment used for these flights was the Mavic 3E Enterprise drone of the DJI brand, a device widely used in high-precision photogrammetric surveys due to the appropriate sensors it equips and its RTK positioning that reduces the uncertainty of its position through real-time corrections by connecting to a GNSS base.

2.1.2. DEVELOPING THE NDSM

After the photogrammetric restitution, a very important product for this research is obtained, which is the DSM (Digital Surface Model) which represents the distribution of heights of the raised surface through photogrammetry techniques, which includes vegetation, vehicles, buildings, terrain and other objects. From this information, a DTM (Digital Terrain Model) can be generated, which seeks to represent only the distribution of terrain heights (excluding objects, vegetation and vehicles) through a classification of the point cloud. The purpose of these products in our research is that by means of an arithmetic difference between these products it is possible to obtain the elevation of the objects, buildings and trees within the study area (Figure 1). The nDSM (normalized surface model) was calculated by subtracting DTM from the DSM (Equation 1)

$$nDSM = DSM - DTM \quad (1)$$

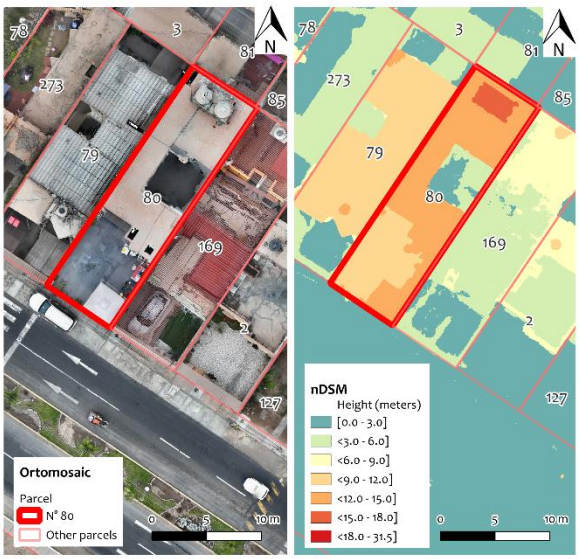

Fig. 2. Visual and elevation information for lot N°80 by photogrammetric products, (a) ortomosaic and (b) normalized DSM (nDSM).

In the nDSM, buildings and other objects may appear to rest on a flat surface. Therefore, they can be identified by analyzing the height values in the nDSM. The nDSM has values ranging from 0 to 31.5, as illustrated in **Figure 2**.

2.1.3. BUILDING HEIGHT ESTIMATION

Based on the elevation values in each raster grid cell, a histogram was generated (Figure 3) to represent the frequency of pixels associated with different height ranges within each lot, as defined by the cadastral map.

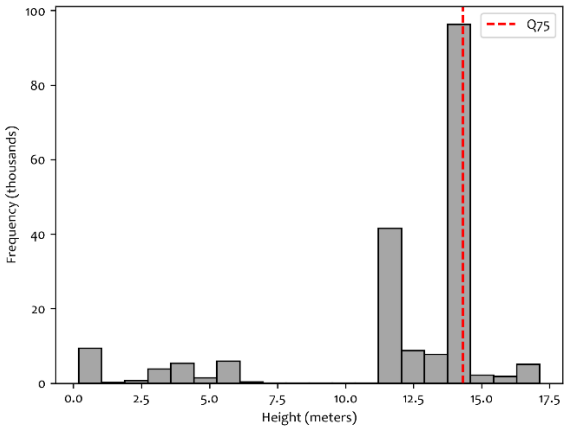

Fig. 3. Height histogram for lot N° 80.

The representative building height within each lot was determined using the 75th percentile value of the pixel distribution. This method reduces the influence of non-structural elements that could distort the actual building height, such as elevated objects on the rooftop (e.g., water tanks or antennas). Then, based on this estimated height, the number of floors was calculated by dividing it by the typical floor height and rounding to the nearest integer using standard rounding rules. A typical floor height of 3 meters was used for this calculation. The building floor values were obtained by using Eq. 2

$$n = round\left(\frac{h}{hf}\right) \quad \ldots (2)$$

Where h is the representative building height, hf is the typical floor height, $round\,(\cdot)$ represents rounding to the nearest integer, and n is the building floor value.

2.2. BUILDING HEIGHT ESTIMATION THROUGH 360 IMAGERIES AT STREET LEVEL

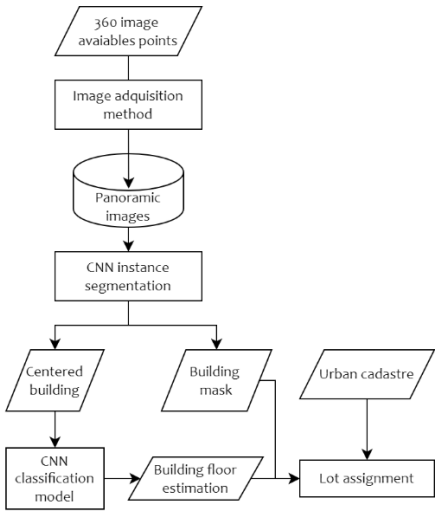

Fig. 4. The framework of the building heights and floor estimation method.

2.2.1. 360 IMAGERY ADQUISITION

For data acquisition, Google Places API and Google Tiles API were used to query all points with available 360-degree images within the study area. These APIs return the location of the nearest point where a panoramic image exists, along with a unique identifier called "pano_id" (see Figure 4).

The set of queried points was generated by subdividing a road network shapefile every 8 meters (which is the approximate spacing between Google Street View images). Figure 5 shows all the available points and the date when the images were captured.

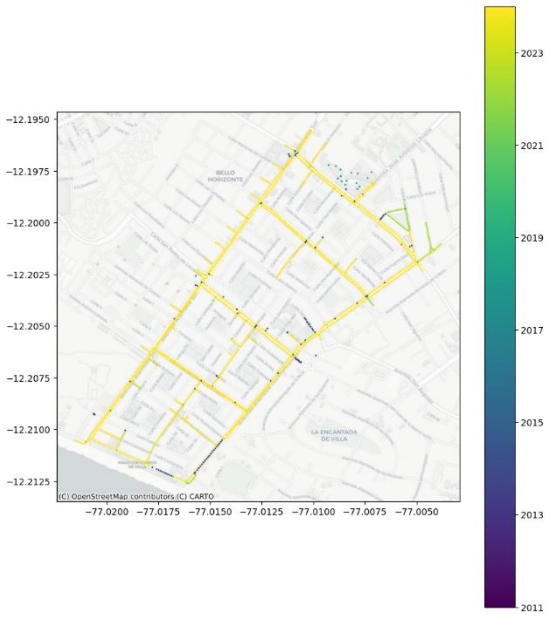

Fig. 5. Available 360 panoramas.

The locations of the obtained 360-degree images are provided in latitude and longitude coordinates using the WGS84 unprojected coordinate system. According to the documentation, these coordinates are not the original ones captured at the time of acquisition but have been adjusted to align with the road network.

To retrieve more detailed parameters for each panorama, Google Tiles API was used. This allowed access to the original capture coordinates, gyroscope information (rotation angles around each capture axis), azimuth, and other relevant metadata.

2.2.2. 360 IMAGERY PREPROCESSING

All tiles for each panorama were generated and merged to reconstruct the complete image. Additionally, each image was corrected using **two** parameters obtained from the associated metadata:

- **Tilt**: The tilt of the panorama, measured in degrees from the south pole of the panorama to the horizon.
- **Roll**: The clockwise rotation around the line of sight that was applied to the panorama to level the horizon.

Due to the urban configuration, where buildings are attached to each other, it is necessary to individually identify each structure. In the study "Automated Building Structural Parameters Extraction for Seismic Risk Assessment in Villa El Salvador Area" [19], several instance segmentation models with classifiers backbones based on Convolutional Neural Networks (CNNs) and Vision Transformers (ViTs) were trained to segment and isolate each building, as shown in Figure 6 and Figure 7.

Fig. 6. Google 360 panorama.

Fig. 7. Segmented buildings.

Fig. 8. Centered building images.

Subsequently, several CNNs were trained to identify five structural parameters related to estimating seismic risk in buildings, one of which is the number of floors (see Figure 8). This parameter will later be used to train a linear regression model to obtain a more accurate prediction value.

2.2.3. PROPERTY ASSIGNMENT

Once the building has been identified and the number of floors classified, the next step involves assigning this value to the cadastral database. This process consists of several steps:

1. The building mask is transformed from a planar projection to its original equirectangular projection (blue polyline).
2. The center of the façade is determined by drawing a horizontal line (red line) approximately 1.5 meters above the base of the mask and finding the midpoint (yellow point) of the intersection, as shown in Figure 9a.
3. After establishing the direction toward the building, it was overlaid onto the cadastre, and the number of floors was assigned to the first lot it intersected.

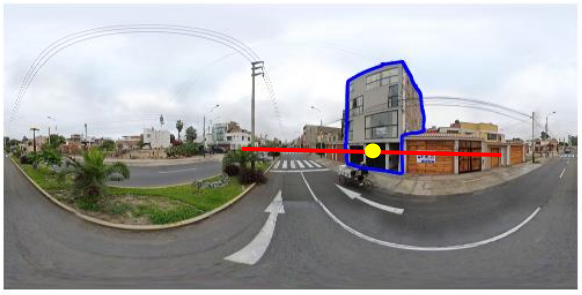

(a)

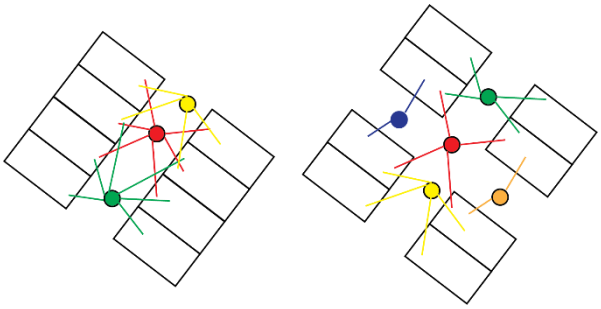

(b)

Fig. 9. (a) Centered building images and (b) Lot assignment.

As shown in Figure 9b, assigning the number of floors to a lot is not unique; rather, it varies depending on the availability of 360-degree images surrounding the building. This situation leads us to propose a method to determine the final assigned value for the number of floors. The proposed equation establishes that if the number of predictions is exactly two, the prediction with the highest probability score should be chosen. If more than two predictions exist, the mode is selected if at least one repetition occurs; otherwise, the prediction with the highest probability is chosen.

$$N_{floors}(N_{preds}) = \begin{cases} argmax(prob_{preds}), & N_{preds} = 2 \\ mode(preds), & N_{preds} > 2 \end{cases} \quad \dots (2)$$

3. STUDY AREA

The study area is in the district of Chorrillos, Lima, Peru. According to the sectorization map extracted from the urban development portal of the district's municipality, it includes three urban developments: "Los Cedros de Villa", "Fovipol" and "Villa del Mar" along with a small section of condominiums.

The total area covers 1.16 km² (Figure 10) and consists of 3,344 lots designated for various uses, including residential, commercial, recreational, educational, and health purposes.

This urban cluster was selected due to its significance for studying damage caused by both earthquakes and tsunamis. According to [20], Chorrillos is the district with the major quantity of dwellings exposed by tsunami inundation in

Metropolitan Lima Area with 51,414 people and 13,912 dwellings exposed to tsunami and the selected urban developments for this study would be completely affected by tsunami inundation [21] under the scenario proposed by Jimenez et al. [22].

Fig. 10. Study area

4. RESULTS ANALYSIS

4.1. COMPARISON OF METHODS

The results of applying both methodologies are visualized in the confusion matrices (Figures 11 and 12). As observed, the CNN-based method fails to identify lots that are vacant land (undeveloped) and is also unable to detect **buildings taller than five floors**.

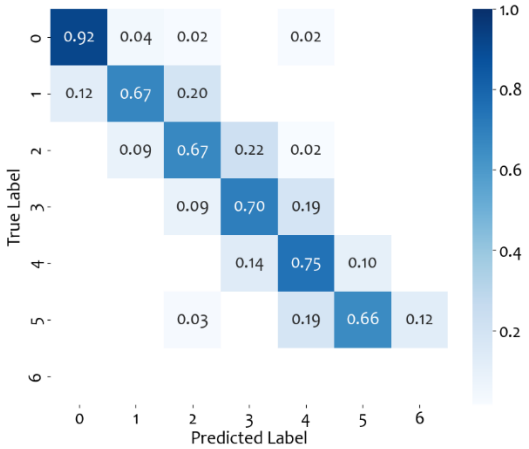

Fig. 11. Normalized confusion matrix with aerial images.

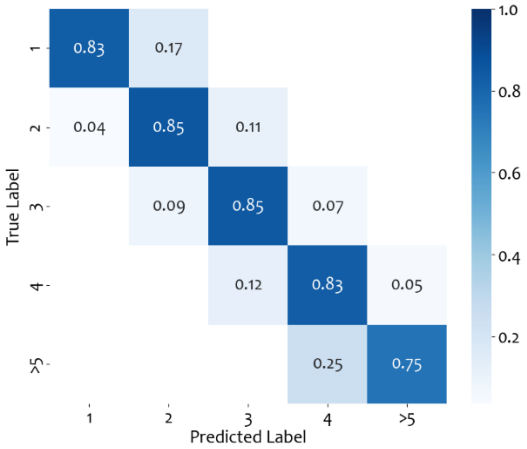

Fig. 12. Normalized confusion matrix with 360 images.

Despite these limitations, the CNN method demonstrates greater accuracy compared to the photogrammetry-based approach. This improvement is primarily because the floor count is based on structural floors, considering:

- Incomplete constructions without a finished roof.
- A floor is counted if at least 50% of its area is built.
- The model ignores upper floors made of lightweight, removable materials such as drywall, wood paneling, Superboard, or other similar materials unless the floor directly below is built with a more resistant material, such as masonry.

4.2. COMBINATION OF METHODS

Since two lists of predicted values are available, a method is proposed to combine them into a new list that will represent the results of both methodologies. This will be achieved through the application of linear regression models.

The training and validation datasets will be obtained by splitting the list of values predicted by the CNN into 80% for training and 20% for validation.

The models used include:

- **Logistic Regression** with a maximum of 1,000 iterations, C = 1, and the lbfgs optimization algorithm.
- **Random Forest** with 100 estimators.
- **Gradient Boosting** with 100 estimators and a learning rate of 0.1.
- **AdaBoost** with 100 estimators and a learning rate of 1.
- **Support Vector Machines** (SVM) with C = 1 and an RBF kernel.

- **k-Nearest Neighbors** (k-NN) with 5 neighbors.
- **Multinomial Naïve Bayes**, specifically designed for discrete data.

Once the proposed regression models were trained, it was verified—according to the performance metrics presented in Table I—that the Random Forest model achieved the best performance, obtaining an accuracy of 0.861. Consequently, the trained model was evaluated on the validation dataset, and the resulting confusion matrix is presented in Figure 13.

TABLA I
Comparison of performance metrics between all linear classification models.

Model	Accuracy	Precision	Recall	F1
Logistic Regression	0.854	0.898	0.844	0.864
Random Forest	**0.861**	0.886	**0.874**	**0.878**
AdaBoost	0.776	0.674	0.566	0.539
SVM	0.856	**0.900**	0.848	0.848
k-NN	0.759	0.832	0.787	0.867
Naive Bayes	0.853	0.868	0.869	0.800

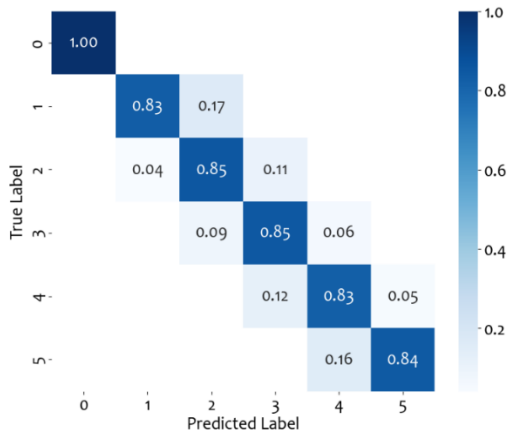

Fig. 13. Normalized confusion matrix with aerial and 360 imagery trained with Random Forest linear regression model.

Table I presents four performance metrics: accuracy, macro precision, recall, and F1-score for each regression model. These values indicate that the Random Forest model achieves the best final fit by utilizing both sources of information: aerial images and street-level panoramic images.

4.3 BUILDING FLOOR COUNT SURVEY USING 3D MODEL

The use of three-dimensional representations for obtaining building information is a widely adopted technique with high accuracy. The most used product for this purpose is the point cloud; however, advancements in drone sensor technology and new data acquisition techniques have enabled the generation of high-quality 3D meshes. This facilitates visual inspections for evaluators using tridimensional models.

In this study, a photogrammetric restitution program was used to generate a 3D mesh in OBJ format from aerial photographs captured by drone. Additionally, this model was shared with surveyors through an online viewer (Figure 14) to determine the number of floors for each building within each lot (see Figure 15).

Fig. 14. Online viewer for tridimensional model.

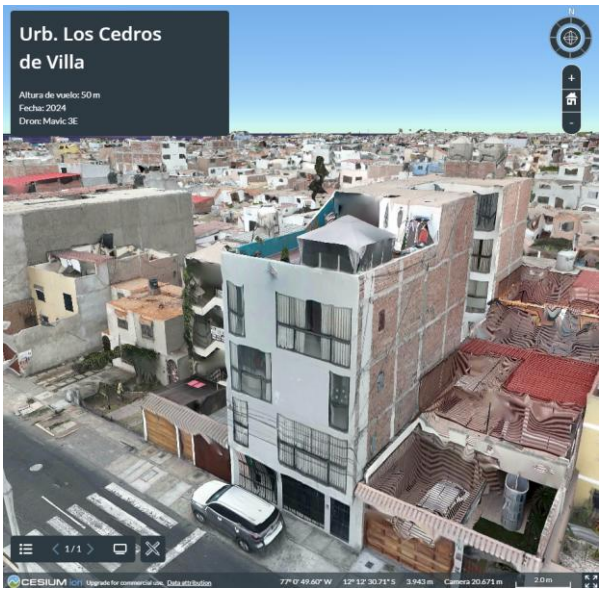

Fig. 15. Tridimensional model for lot N°80.

5. SEISMIC ASSESTMENT

The seismic risk assessment considered three seismic demand levels: severe, rare, and very rare [23], corresponding to average return periods of 475, 975, and 2,475 years (with 10%, 5%, and 2% probabilities of exceedance in 50 years).

Based on the Peruvian Earthquake-Resistant Design Standard (NTE-E030-2018)[24], these scenarios resulted in maximum ground accelerations of 441, 574, and 662 cm/s² on rigid soil profiles, respectively. Soil amplification factors for the study area were applied to estimate surface-level accelerations.

Risk estimation was performed using SRSND software by Zavala et al [25], previously validated with damage data from the 2007 Pisco Earthquake . Risk was quantified as repair costs relative to original building costs, calibrated using observed damages from the Pisco event. Additional vulnerability studies by CISMID refined these repair-cost thresholds [26, 27, 28]. Table II summarizes the risk classification based on and Figure 16 shows the spatial distribution of seismic risk according to the three levels of demand.

TABLE II
Classification of risk levels based on estimated repair cost.

Model	Repair cost	Associated damage
Level 1	<15%	No damage, slight damage
Level 2	15% - 30%	Light damage
Level 3	30% - 60%	Moderate damage
Level 4	60% - 85%	Severe damage
Level 5	>85%	Collapse

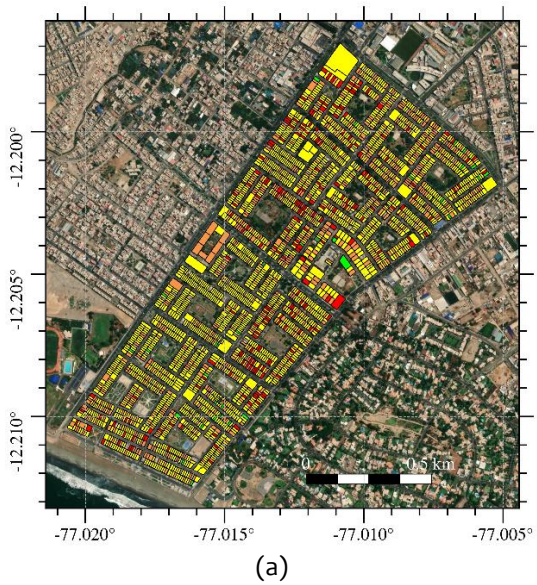

(a)

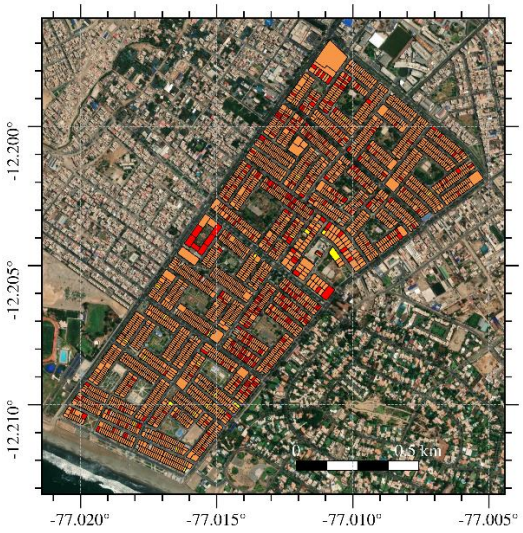

(b)

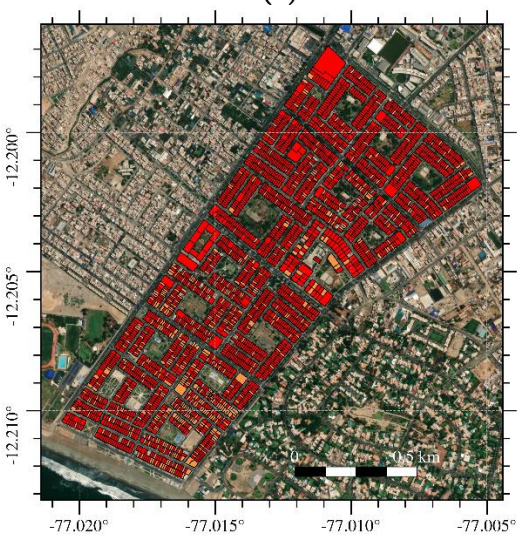

(c)

Fig. 16. Spatial distribution of seismic risk at the lot level. a) Tr=475 years, b) Tr=975 years, and c) 2475 years.

6. CONCLUSIONS

Photogrammetric restitution from aerial photographs captured by drones is a cost-effective, fast, and accurate technique compared to other building survey methods. This approach is particularly useful for the development of urban inventories aimed at various fields, such as Disaster Risk Management, where spatial information and building characteristics are key factors in determining risk levels.

Using the method based on photogrammetric products, the highest accuracy was obtained for vacant land (92%), while the lowest accuracy was observed in five-story buildings (66%).

Using the CNN method based on 360 imageries at street level, the highest accuracy was obtained for two-story and three-story buildings (85%), while the lowest accuracy was observed in five-story buildings or tallest (75%).

Combining both methods, the highest accuracy was obtained for vacant land buildings (100%), while the lowest accuracy was observed in one-story and three-story buildings (83%).

ACKNOWLEDGEMENTS

This study was conducted within the framework of the SATREPS project, entitled "Development of an Integrated Expert System for the Estimation and Observation of Damage Levels in Infrastructure in the Metropolitan Area of Lima". The authors would like to thank the Japan Science and Technology Agency (JST) and the Japan International Cooperation Agency (JICA) for sponsoring and donating a geodetic receiver and drone used in this project.

REFERENCES

[1] A. Erener, G. Sarp, and M. I. Karaca, "An approach to urban building height and floor estimation by using LiDAR data," *Arabian Journal of Geosciences*, vol. 13, no. 19, p. 1005, 2020, doi: 10.1007/s12517-020-06006-1.

[2] X. Ma and others, "Mapping fine-scale building heights in urban agglomeration with spaceborne lidar," *Remote Sensing of Environment*, vol. 285, p. 113392, 2023, doi: 10.1016/j.rse.2022.113392.

[3] J. Lao and others, "Retrieving building height in urban areas using ICESat-2 photon-counting LiDAR data," *International Journal of Applied Earth Observation and Geoinformation*, vol. 104, p. 102596, 2021, doi: 10.1016/j.jag.2021.102596.

[4] I. da Silva, W. Ibañez, and G. Poleszuk, "Experience of Using Total Station and GNSS Technologies for Tall Building Construction Monitoring," in *Facing the Challenges in Structural Engineering*, H. Rodrigues, A. Elnashai, and G. M. Calvi, Eds., Cham: Springer International Publishing, 2018, pp. 471–486.

[5] G. Liasis and S. Stavrou, "Satellite images analysis for shadow detection and building height estimation," *ISPRS Journal of Photogrammetry and Remote Sensing*, vol. 119, pp. 437–450, 2016, doi: 10.1016/j.isprsjprs.2016.07.006.

[6] X. Li, Y. Zhou, P. Gong, K. C. Seto, and N. Clinton, "Developing a method to estimate building height from Sentinel-1 data," *Remote Sensing of Environment*, vol. 240, p. 111705, 2020, doi: 10.1016/j.rse.2020.111705.

[7] M. Liu, P. Wang, K. Hu, C. Gu, S. Jin, and L. Chen, "A Method for Extracting High-Resolution Building Height Information in Rural Areas Using GF-7 Data," *Sensors*, vol. 24, no. 18, 2024, doi: 10.3390/s24186076.

[8] F. Qi, J. Z. Zhai, and G. Dang, "Building height estimation using Google Earth," *Energy and Buildings*, vol. 118, pp. 123–132, 2016, doi: 10.1016/j.enbuild.2016.02.044.

[9] Y. Cao and X. Huang, "A deep learning method for building height estimation using high-resolution multi-view imagery over urban areas: A case study of 42 Chinese cities," *Remote Sensing of Environment*, vol. 264, p. 112590, 2021, doi: 10.1016/j.rse.2021.112590.

[10] Y. Yan and B. Huang, "Estimation of building height using a single street view image via deep neural networks," *ISPRS Journal of Photogrammetry and Remote Sensing*, vol. 192, pp. 83–98, 2022, doi: 10.1016/j.isprsjprs.2022.08.006.

[11] Z. Xu, F. Zhang, Y. Wu, Y. Yang, and Y. Wu, "Building height calculation for an urban area based on street view images and deep learning," *Computer-Aided Civil and Infrastructure Engineering*, vol. 38, no. 7, pp. 892–906, 2023, doi: 10.1111/mice.12906.

[12] CISMID, "Estudio de microzonificación sísmica y evaluación de la vulnerabilidad de edificaciones en el distrito de Villa El Salvador, Lima," Universidad Nacional de Ingeniería, Lima, Perú, Informe técnico, 2011.

[13] B. Adriano *et al.*, "Tsunami Inundation Mapping in Lima, for Two Tsunami Source Scenarios," *Journal of Disaster Research*, vol. 8, no. 2, pp. 274–284, 2013, doi: 10.20965/jdr.2013.p0274.

[14] R. Iskandar *et al.*, "Estimating urban seismic damages and debris from building-level simulations: application to the city of Beirut, Lebanon," *Bulletin of Earthquake Engineering*, vol. 21, no. 13, pp. 5949–5990, Oct. 2023, doi: 10.1007/s10518-023-01768-x.

[15] E. Berny, C. Avelar, M. A. Salgado-Gálvez, and M. Ordaz, "Estimating emergency costs for earthquakes and floods in Central Asia based on modelled losses," *Natural Hazards and Earth System Sciences*, vol. 24, no. 1, pp. 53–62, 2024, doi: 10.5194/nhess-24-53-2024.

[16] Peter Drenan and Shandi Treloar, "Debris Estimation and Forecasting Tools and Approaches," in *A Debris Management Handbook for State and Local DOTs and Departments of Public Works*, National Academies of Sciences, Engineering, and Medicine, Ed., Washington, DC: The National Academies Press, 2014, pp. 14–20. doi: 10.17226/22239.

[17] J. Li, X. Huang, L. Tu, T. Zhang, and L. Wang, "A review of building detection from very high resolution optical remote sensing images," *GIScience and Remote Sensing*, vol. 59, no. 1. Taylor and Francis Ltd., pp. 1199–1225, 2022. doi: 10.1080/15481603.2022.2101727.

[18] M. Buyukdemircioglu, R. Can, S. Kocaman, and M. Kada, "DEEP LEARNING BASED BUILDING FOOTPRINT EXTRACTION FROM VERY HIGH RESOLUTION TRUE ORTHOPHOTOS AND NDSM," in *ISPRS Annals of the Photogrammetry, Remote Sensing and Spatial Information Sciences*, Copernicus GmbH, May 2022, pp. 211–218. doi: 10.5194/isprs-annals-V-2-2022-211-2022.

[19] J. Salinas, M. Diaz, C. Zavala, M. Matsuoka, I. Inocente, and F. Garcia, "Automated Building Structural Parameters Extraction for Seismic Risk Assessment in Villa El Salvador Area," *JDR*, vol. 20, no. 6, pp. 959–974, Dec. 2025, doi: 10.20965/jdr.2025.p0959.

[20] CENEPRED, "Escenario de riesgo por sismo y tsunami para Lima y Callao." Dec. 2020. [Online]. Available: https://sigrid.cenepred.gob.pe/sigridv3/storage/biblioteca//10354_escenario-de-riesgo-por-sismo-y-tsunami-para-lima-y-callao.pdf

[21] A. Quesquen, M. Estrada, F. Garcia, C. Davila, B. Puchoc, and S. Koshimura, "Systematization of geospatial information of urban occupation in Metropolitan Lima-Callao for the evaluation of the tsunami threat by different seismic scenarios," 2025.

[22] C. Jimenez *et al.*, "Seismic Source of 1746 Callao Earthquake from Tsunami Numerical Modeling," *Journal of Disaster Research*, vol. 8, no. 2, pp. 266–273, 2013, doi: 10.20965/jdr.2013.p0266.

[23] M. Diaz, C. Zavala, M. Estrada, and M. Matsuoka, "Characterization of the Structural Typologies of Buildings in the Lima Metropolitan Area," *Journal of Disaster Research*, vol. 18, no. 4, pp. 329–337, June 2023, doi: 10.20965/jdr.2023.p0329.

[24] SENCICO, "Technical Standard of Buildings E.030: Earthquake-resistant Design." 2018.

[25] C. Zavala, Z. Aguilar, and M. Estrada, "Evaluation of SRSND simulator against fragility curves for Pisco Quake," in *8th Center for Urban Earthquake Engineering Conference*, Tokyo, Japan, Mar. 2011.

[26] CISMID, "ESTUDIOS DE MICROZONIFICACIÓN GEOTÉCNICA SÍSMICA Y EVALUACIÓN DEL RIESGO EN ZONAS UBICADAS EN LOS DISTRITOS DE CARABAYLLO Y EL AGUSTINO (PROVINCIA Y DEPARTAMENTO DE LIMA); DISTRITO DEL CUSCO (PROVINCIA Y DEPARTAMENTO DEL CUSCO); Y DISTRITO DE ALTO SELVA ALEGRE (PROVINCIA Y DEPARTAMENTO DE AREQUIPA)," Universidad Nacional de Ingeniería, Lima, Perú, Informe técnico, 2013.

[27] CISMID, "CONVENIO DE COLABORACIÓN INTERINSTITUCIONAL ENTRE EL MINISTERIO DE VIVIENDA, CONSTRUCCIÓN Y SANEAMIENTO Y LA UNIVERSIDAD NACIONAL DE INGENIERÍA PARA LA ELABORACIÓN DE LOS ESTUDIOS DE MICROZONIFICACIÓN SÍSMICA Y ANÁLISIS DE RIESGO EN ZONAS DE ESTUDIOS UBICADAS EN LAS ÁREAS URBANAS DE LAS MUNICIPALIDADES DISTRITALES DE PUEBLO LIBRE (LIMA), LA VICTORIA (LIMA), TRUJILLO (LA LIBERTAD) Y VÍCTOR LARCO HERRERA (LA LIBERTAD).," Universidad Nacional de Ingeniería, Lima, Perú, Informe técnico, 2018.

[28] CISMID, "ANÁLISIS DE RIESGO EN ZONAS URBANAS DEL DISTRITO DE SAN ISIDRO," Universidad Nacional de Ingeniería, Lima, Perú, Informe técnico, 2019.